molecules

MDPI

Article

Impact of Impure Gas on CO_2 Capture from Flue Gas Using Carbon Nanotubes: A Molecular Simulation Study

Yiru Su [1,2], Siyao Liu [1,*] and Xuechao Gao [3,*]

[1] Key Laboratory of Low-Grade Energy Utilization Technologies and Systems, Ministry of Education, School of Energy and Power Engineering, Chongqing University, Chongqing 400044, China; sophia_yiru@163.com
[2] State Key Laboratory of Pollution Control and Resource Reuse, School of the Environment, Nanjing University, Nanjing 210023, China
[3] State Key Laboratory of Materials-Oriented Chemical Engineering, College of Chemical Engineering, Nanjing Tech University, Nanjing 211816, China
* Correspondence: siyaoliu@cqu.edu.cn (S.L.); xuechao.gao@njtech.edu.cn (X.G.)

Abstract: We used a grand canonical Monte Carlo simulation to study the influence of impurities including water vapor, SO_2, and O_2 in the flue gas on the adsorption of CO_2/N_2 mixture in carbon nanotubes (CNTs) and carboxyl doped CNT arrays. In the presence of single impure gas, SO_2 yielded the most inhibitions on CO_2 adsorption, while the influence of water only occurred at low pressure limit (0.1 bar), where a one-dimensional chain of hydrogen-bonded molecules was formed. Further, O_2 was found to hardly affect the adsorption and separation of CO_2. With three impurities in flue gas, SO_2 still played a major role to suppress the adsorption of CO_2 by reducing the adsorption amount significantly. This was mainly because SO_2 had a stronger interaction with carbon walls in comparison with CO_2. The presence of three impurities in flue gas enhanced the adsorption complexity due to the interactions between different species. Modified by hydrophilic carboxyl groups, a large amount of H_2O occupied the adsorption space outside the tube in the carbon nanotube arrays, and SO_2 produced competitive adsorption for CO_2 in the tube. Both of the two effects inhibited the adsorption of CO_2, but improved the selectivity of CO_2/N_2, and the competition between the two determined the adsorption distribution of CO_2 inside and outside the tube. In addition, it was found that (7, 7) CNT always maintained the best CO_2/N_2 adsorption and separation performance in the presence of impurity gas, for both the cases of single CNT and CNT array.

Keywords: molecular simulation; gas separation; single-walled carbon nanotube; impure gases

check for updates

Citation: Su, Y.; Liu, S.; Gao, X. Impact of Impure Gas on CO_2 Capture from Flue Gas Using Carbon Nanotubes: A Molecular Simulation Study. *Molecules* **2022**, *27*, 1627. https://doi.org/10.3390/molecules27051627

Academic Editor: Susana Valencia

Received: 14 December 2021
Accepted: 31 January 2022
Published: 1 March 2022

1. Introduction

Carbon capture and storage (CCS) [1] technologies have been extensively developed to minimized the influence of CO_2 emission on the global warming effect. Among the separation techniques, adsorption separation [2] is regarded as a promising solution for its low cost and high efficiency. In this connection, a host of conventional and emerging nanoporous materials have been invented and explored, including zeolites, activated carbons, metal-organic frameworks (MOFs), and carbon nanotubes (CNTs) [3–8]. Particularly, CNTs possess large specific surface areas (greater than 1000 m^2/g) with strong adsorptive affinities, which could be paired with the superior transport properties to further facilitate the adsorption potentials of [3,9–24] CNTs for CO_2 capture.

In our previous study, grand canonical Monte Carlo (GCMC) simulations were conducted to investigate the adsorption of CO_2 in the internal space of individual single CNTs in the presence of pre-adsorbed water [3]. It was found that the pre-loaded water provided additional H_2O–CO_2 interactions to facilitate the adsorption of CO_2, by taking up the adsorption site available for CO_2. Similarly, as reported by Yu et al. [1], the presence of SO_2 in the gas phase exerted a negative effect on the adsorption of CO_2 for $CO_2/N_2/SO_2$ mixture

in HKUST-1 at ambient temperature. By comparison, the presence of O_2 exerted little effect on the adsorption of CO_2 in HKUST-1. The main components of flue gases generated by coal-fired power plants include N_2 (about 73–77%), CO_2 (15–16%), H_2O (5–7%), O_2 (about 3–4%) [12], and trace amounts of SO_2, etc. [25,26]. Therefore, the impurity gases, such as H_2O, O_2, and SO_2 are expected to impose a significant influence on the adsorption and separation of CO_2 from flue gas using CNTs [1,3,27–30].

In practice, oxidation defects often occurred during the acidic/oxidative purification of carbon nanotubes [31], where oxygen-containing functional groups (mainly carbonyl and carboxyl) could be grafted to the defect sites [32]. The oxygen-containing functional groups, such as carboxyl and hydroxyl groups, are hydrophilic, so it could significantly enhance the adsorption of water vapor contained in flue gas, which thus imposes strong influence on the adsorption in CNTs for the rest components in flue gas [33,34]. Further, instead of single carbon nanotube, carbon nanotube bundles were generally obtained during the synthesis procedure. Therefore, to explore the influence of impurity gases on the adsorption and separation of CO_2 from flue gas in a practical manner, the adsorption of gas mixtures ($CO_2/N_2/X$, X denotes the impurity gases, H_2O, SO_2, and O_2) in the functionalized CNT bundles are required. To the best of our knowledge, the adsorption behavior of impurity gases in the functionalized CNT bundles is still unknown. Hence, the effects of three impurity gases on the separation of CO_2 in CNT also have not been systematically studied. Different from binary mixture, there are more complex interactions between three impurity gases, the cooperative impact on CO_2 adsorption has hardly been studied. In addition, little is known about how the cooperative effects between adsorbate-CNT interaction and interaction between impurity and adsorbate affect CO_2/N_2 selectivity. Discussions related to these and other related issues will be obtained in detail in this work. Furthermore, the influence on the optimum diameter of CNTs for separating CO_2/N_2 is not reported yet.

In this work, GCMC and density functional theory (DFT) simulations were conducted to investigate the adsorption separation of CO_2 from flue gases using carbon nanotubes in the presence of impurity species (H_2O, O_2 and SO_2), in order to fundamentally reveal the impacts of impurity gases on the adsorption behaviors and separation performance of CO_2. DFT calculations were specifically conducted to add the carboxyl groups to the vacant oxidation defects of CNTs. Both the adsorption of gas mixtures in single carbon nanotubes and carbon nanotube bundles with functional groups were systematically considered. The separation of SO_2/N_2 mixtures also was investigated in CNTs. As both adsorption capacity and selectivity determine the performance of the adsorbents, the performance coefficient of functionalized CNT bundles was used to comprehensively evaluate the CO_2 separation potential using CNTs.

2. Simulation Details

2.1. Molecular Models

In our simulations, CO_2 was modeled by EMP2 model of Harris and Yung [35]. N_2 and O_2 were treated as a rigid three-site model with two LJ sites carrying negative charges to represent the N/O atoms, associated with a dummy particle located at center of mass (COM) being used to carry the positive charges to maintain the electrostatic neutralization of molecule [36]. H_2O was represented by the SPC/E model, which treated H_2O as a rigid molecule with a positive charges on H atoms and negative partial charges on the O atom [37]. SO_2 is modeled as a three-site model as well, with a charged LJ particle being assigned for each atom [38]. In addition, the Steele parameters were used to represent the carbon atoms in CNTs. All of the configurational parameters [13], LJ parameters, and partial charges of these guest molecules and the CNTs are summarized in Table 1. The adsorption configuration of gas molecules in four CNTs, the optimized structure of CNT unit cell with defects, and the constructed CNT array can be seen in Figure 1a,b.

The interactions of adsorbate–adsorbent and adsorbate–adsorbate are described by the dispersion and electrostatic terms, given by

$$u_{ij}^{(\alpha,\beta)} = 4_{ij}^{(\alpha,\beta)} \left[\left(\frac{\sigma_{ij}^{(\alpha,\beta)}}{r_{ij}^{(\alpha,\beta)}} \right)^{12} - \left(\frac{\sigma_{ij}^{(\alpha,\beta)}}{r_{ij}^{(\alpha,\beta)}} \right)^{6} \right] + \frac{1}{4\pi\varepsilon_0} \frac{q_i q_j}{r_{ij}^{(\alpha,\beta)}} \quad (1)$$

where $r_{ij}^{(\alpha,\beta)}$ is the distance between the atom i and j of molecules α and β. The LJ size parameter σ_{ij} and well depth parameter ε_{ij} for the interactions between different species were estimated using Lorentz–Berthelot mixing rules [39], and the Dot Line Method was used to modify the long range electrostatic interactions in CNTs [40,41].

Table 1. Lennard–Jones parameters, partial charges, and configurational parameters of adsorbates and CNT [1].

Molecule	Site	LJ Parameters		Molecular Model			
		$\varepsilon/k_B(K)$	$\sigma(nm)$	X(nm)	Y(nm)	Z(nm)	Charge (e)
CNT	C	28.0	0.34				0.000
	C, H	35.220	0.355				−0.115
	C, RCOOH	52.840	0.375				0.520
	O(C), RCOOH	105.68	0.296				−0.440
	O(H),RCOOH	85.550	0.300				−0.530
	H, RCOOH	0.00015	0.000				0.450
	H, RC	100	0.242				0.115
CO_2	C	27.0	0.280	0.0	0.0	0.0	0.70
	O	79.0	0.305	±0.1149	0.0	0.0	−0.35
N_2	N	36.0	0.331	±0.055	0.0	0.0	−0.482
	COM	0	0	0.0	0.0	0.0	0.964
H_2O	O	78.2	0.317	0.0	0.0	0.0	−0.848
	H	0	0	±0.0765	0.0	0.0587	0.424
O_2	O	54.4	0.305	±0.0604	0.0	0.0	−0.112
	COM	0	0	0.0	0.0	0.0	0.224
SO_2	O	57.4	0.301	±0.1235	0.0	0.0	−0.235
	S	145.9	0.362	0.0	0.0	0.0	0.471

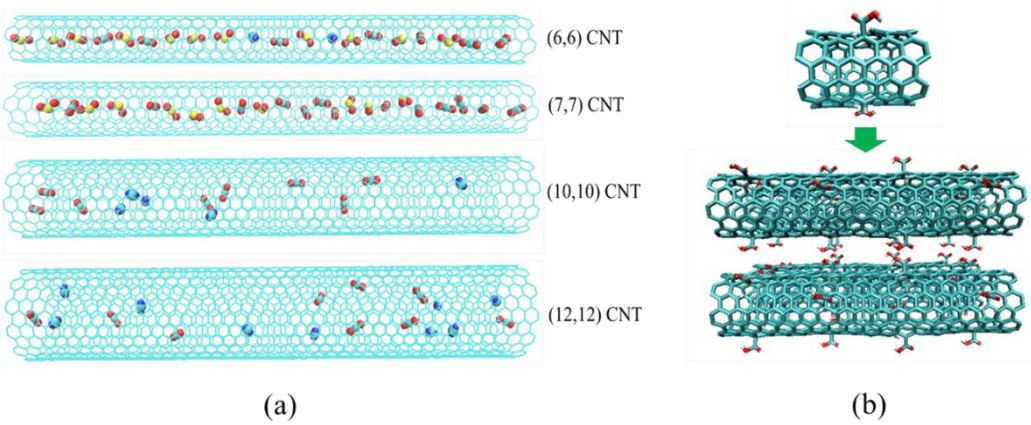

Figure 1. Snapshots of the adsorption of CO_2/N_2 mixture in four CNTs in the presence of impurities, at 1.0 bar and 300 K, where the blue and cyan spheres used for N_2 molecules, while the red and cyan spheres were for CO_2 molecules, and O_2 molecules were marked as the red and yellow spheres (e.g., Red = oxygen, yellow = sulfur, cyan = carbon, blue = nitrogen) (**a**). The optimized structure of CNT unit cell with defects, and the constructed 2 × 2 CNT array (**b**).

2.2. Grand Canonical Monte Carlo Simulations

To gain insights of the effect of impure gases on the adsorptive separation of CO_2 from flue gas using CNTs, three impurity gases, SO_2, H_2O, and O_2, were used to conduct simulations for the adsorption in four different CNTs ((6, 6), (7, 7), (10, 10) and (12, 12)), having the diameters of 0.81 to 1.63 nm, were considered. Initially, the adsorption of binary mixture CO_2/N_2 in different CNTs was examined to find out the optimized pore size of the CNT for CO_2 separation. Afterwards, ternary mixtures, including $CO_2/N_2/SO_2$, $CO_2/N_2/O_2$, and $CO_2/N_2/H_2O$ were used to determine the effects of individual single impurity on the separation performance of CNTs. Eventually, the simulations for the adsorption of quinary mixture, $CO_2/N_2/SO_2/H_2O/O_2$ was conducted to reveal the effect of the co-existing impure gases on the CO_2 separation, and the optimal CNT pore size for CO_2 separation in practice. In all the simulations, the molar ratio of CO_2/N_2 mixture was fixed at 16/84 in the bulk phase, while the partial pressure of H_2O in the ternary mixtures being set as at its saturation pressure of 3.537 kPa, at 300 K. In addition, the mole fraction of SO_2 and O_2 in the ternary mixture was set as 0.08% and 4%, respectively. However, for the quinary mixture, the mole fractions of each gas species were defined as: 16 CO_2: 4 O_2: 3.16 H_2O: 0.08 SO_2 [17], which were chosen to mimic the practical composition of flue gases.

GCMC simulations were conducted to measure the adsorption and separation of CO_2 from flue gas in consideration of the effects of impurities, the adsorbate chemical potential μ, system volume V, and temperature T were maintained constant during simulations. Three Monte Carlo trial moves including the displacement, insertion, and deletion with corresponding probabilities of 0.4, 0.3, and 0.3 were implemented. The fugacities of the components in the bulk phases were calculated using the Peng–Robinson equation of state [42] (PR EOS) for mixtures. For the binary mixture, 1×10^7 configurations were used to equilibrate the system, which was supplemented by another 5×10^7 configurations for statistical analysis. For the ternary mixtures, the configurations used for equilibration and statistics become 1×10^8 and 2×10^8, respectively. For the quinary mixture, $3 \times 10^8$and 6×10^8 configurations were used for equilibration and measuring the isotherm measurement. The equilibrium selectivity, S_{ij}, was calculated according to

$$S_{i/j} = \left(\frac{x_i}{y_i}\right) / \left(\frac{x_j}{y_j}\right) \tag{2}$$

where, x_i and y_i were the molar fractions of component i in the adsorbed and bulk phases, respectively.

Four kinds of CNTs with different diameters were doped with carboxyl groups to form CNT bundles. Firstly, the original unit cell of carbon nanotube model was established. Carbon atoms were randomly deleted to produce a vacant defect, where each vacant defect contained three sp3 hybrid carbon atoms. The carboxyl group was randomly grafted to one of the SP^3 hybrid carbon atoms, and hydrogen atoms were added to the other two carbon atoms to saturate the free valence. After the three vacancy defects were modified, the cell was randomly rotated and spliced three times to form a supercell, to derive the original structure of functionalized CNTs. Then, the density functional theory (DFT) was used to optimize the structure to derive the best geometry. The DFT calculation was conducted in Vienna ab initio simulation package (VASP) software package, where Perdew Burke ernzerhof (PBE) [43] was used as the exchange correlation function and a plane-wave cutoff energy was set to be 550 eV. The optimized structure was used to construct 2×2 carbon nanotube arrays, where the inter-tube distance was maintained at 0.6 nm. The simulation box containing CNT bundles has dimensions of $38 \times 38 \times 50$ Å, and the periodic boundary conditions were applied in the x and y directions.

3. Results and Discussion

3.1. Effect of Pore Size on the Adsorption of CO_2/N_2 Mixture in CNTs

The adsorption of CO_2/N_2 mixture (with a mole ratio of 16/84 in the gas phase) in the CNTs at 300 K is conducted to derive the optimal diameter for CO_2 capture, where the pore diameters varies from 0.81 to 1.63 nm. Figure 2 depicts the adsorption isotherms of CO_2/N_2 and the corresponding CO_2/N_2 selectivity at 300 K. As suggested, within the diameter range, all the adsorption isotherms of CO_2 and N_2 could be represented by type I according to the IUPAC classification. It is seen that the adsorption of CO_2 and the CO_2/N_2 selectivity in the (6, 6) CNT with a diameter of 0.81 nm achieves their maxima below 1.0 bar. However, for the pressure range from 1.0 to 5.0 bar, the (7, 7) CNT with a diameter of 0.95 nm exhibits superior performance on separation CO_2/N_2 in comparison with the performance in the rest, in which both the adsorption of CO_2 and the CO_2/N_2 selectivity are the highest. In the larger (10, 10) and (12, 12) CNTs, although the adsorption amount of CO_2 monotonically increases with pressure, which is consistently higher than the result in the small CNT, the CO_2/N_2 selectivity is dramatically reduced compared with the value in the (6, 6) and (7, 7) CNTs. Consequently, the enlarged CNT diameter promotes the adsorption capacity of CO_2 and N_2 simultaneously, while reducing the CO_2/N_2 selectivity for the weak adsorbate–adsorbent interactions. Considering the superior adsorption amount of CO_2 and significantly higher CO_2/N_2 selectivity, the (6, 6) and (7, 7) CNTs can provide great potential on CO_2 separation from flue gas.

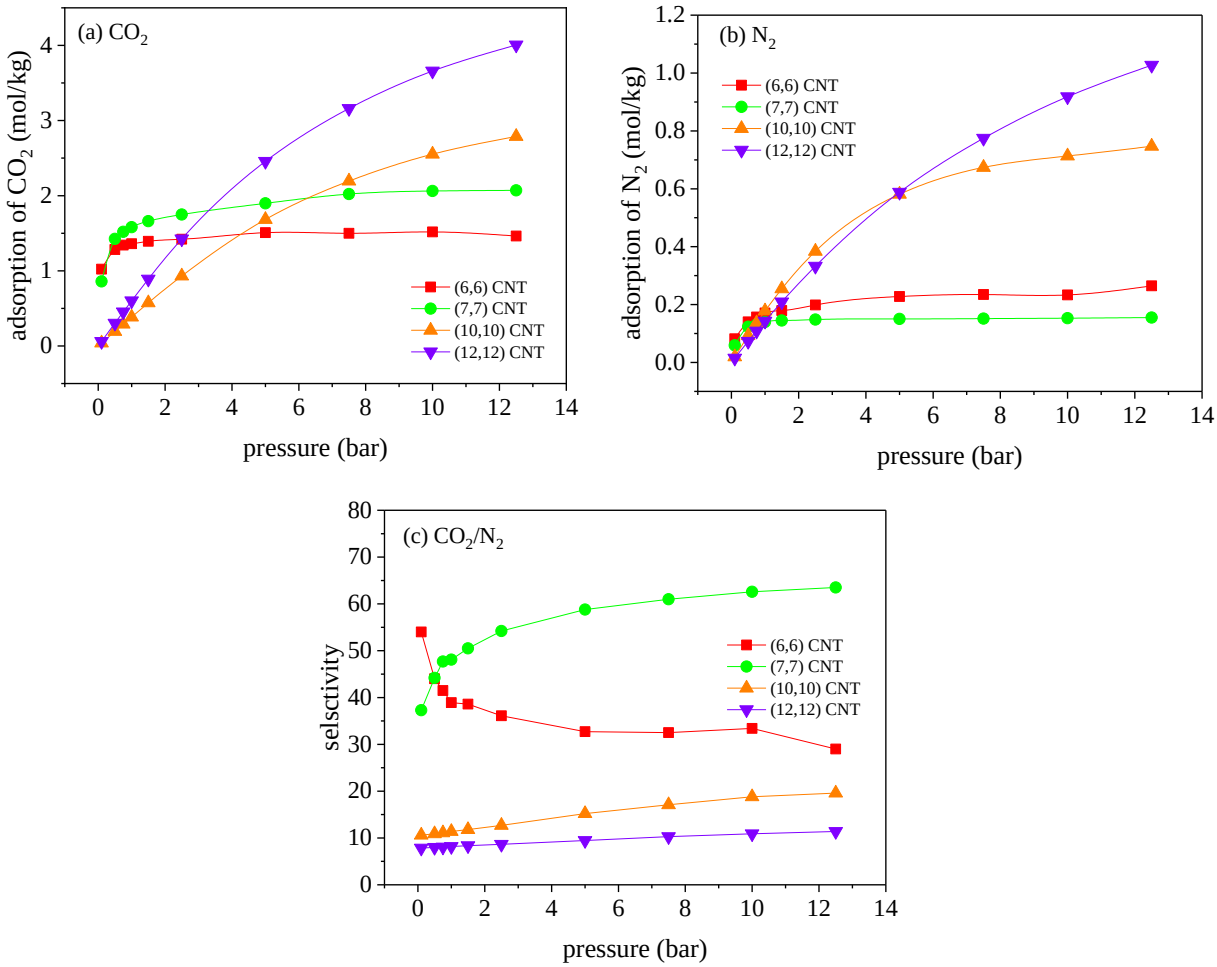

Figure 2. Adsorption isotherms of (**a**) CO_2 and (**b**) N_2, and (**c**) the variation of the corresponding CO_2/N_2 selectivity with pressure in different CNTs, at 300 K.

It is understood that the adsorption of CO_2/N_2 mixture in the CNTs is determined by the competition effect between the adsorbate–adsorbent interactions and the entropic effect. Figure 3 illustrates the variation of CO_2–CNT and N_2–CNT interactions with pressures in the CNTs with different pore sizes, where the detailed calculating procedure was provided in our previous study [3]. Although both the CO_2–CNT and N_2–CNT interactions decrease with the pore size of CNTs, the dependency of interactions on the pore size is stronger for CO_2. Accordingly, the preferential adsorption of CO_2 over N_2 is suppressed in the larger CNTs, leading to the reduced CO_2/N_2 selectivity. In consideration of the nominal diameter, d_{CNT}, of the (6, 6) CNT is 0.81 nm, the effective diameter for CO_2 molecules rotating inside the (6, 6) CNT can be approximately measured as $d_{eff} = d_{CNT} - \sigma_{O-C} = 0.49$ nm, where $\sigma_{O-C} = 0.32$ nm is determined according to $(\sigma_o + \sigma_C)/2$, using the LJ size parameters of carbon atoms (σ_C) of the CNT and oxygen atom (σ_O) of the CO_2 molecule. As the molecule size of CO_2 molecule (0.5331 nm) in the axial direction is larger and that for N_2 molecule (0.441 nm), CO_2 molecules in our simulations are found to distribute almost in parallel to the axis of the (6, 6) CNT, showing strong rotational restrictions. However, the rotational freedom of N_2 is negligibly affected. In addition, random distributions of CO_2 molecules are observed in the (7, 7) CNT with a diameter of 0.95 nm, suggesting that the dramatically enhanced entropic effect is responsible for the reduced CO_2/N_2 selectivity in the (6, 6) CNT, compared to the (7, 7) CNT.

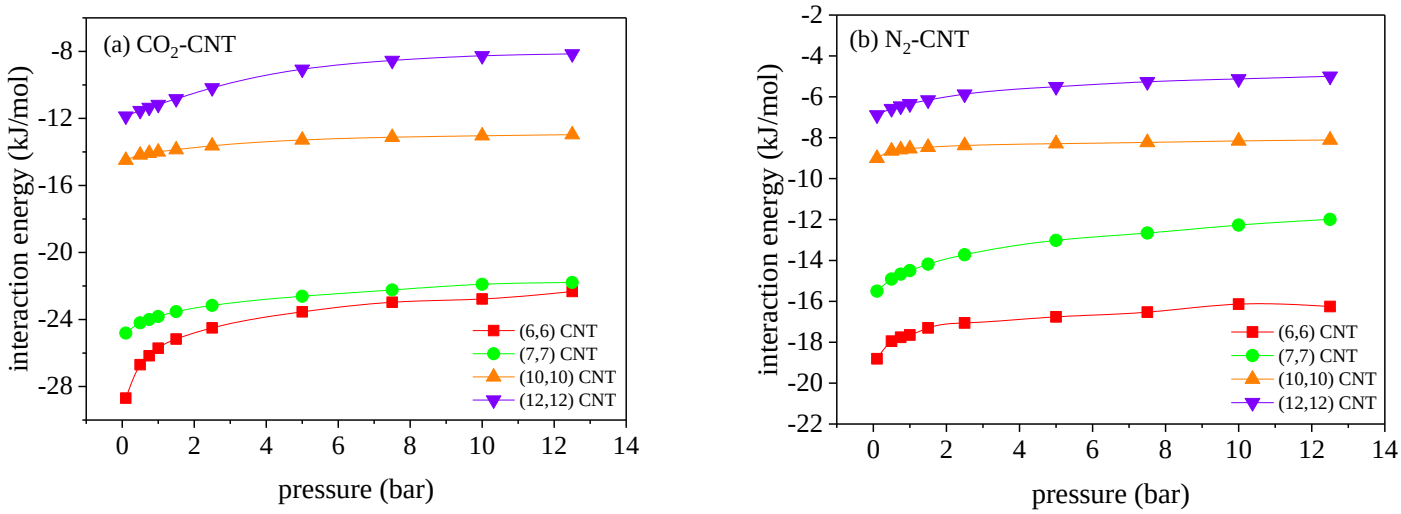

Figure 3. Variation of the interaction energies of (**a**) CO_2-CNT and (**b**) N_2-CNT with pressure, at 300 K.

3.2. Effect of Single Impurity on the Adsorption of CO_2/N_2 Mixtures in CNTs

The adsorption of ternary mixtures, $CO_2/N_2/X$ in CNTs at 300 K, with X denoting a specific impure gas including H_2O, SO_2, and O_2, is further investigated. It is found that insignificant impact of impurities on the separation of CO_2 is found in the (10, 10) and (12, 12) CNTs in all the cases, so all the simulation results for the (10, 10) and (12, 12) CNTs are provided in Figure S1 in the Supporting Information, and the results for the (6, 6) and (7, 7) CNTs are explored. The results for the adsorption of CO_2 and CO_2/N_2 selectivity in these two CNTs are plotted in Figure 4. The adsorption curves of three impurities are shown in Figure S2.

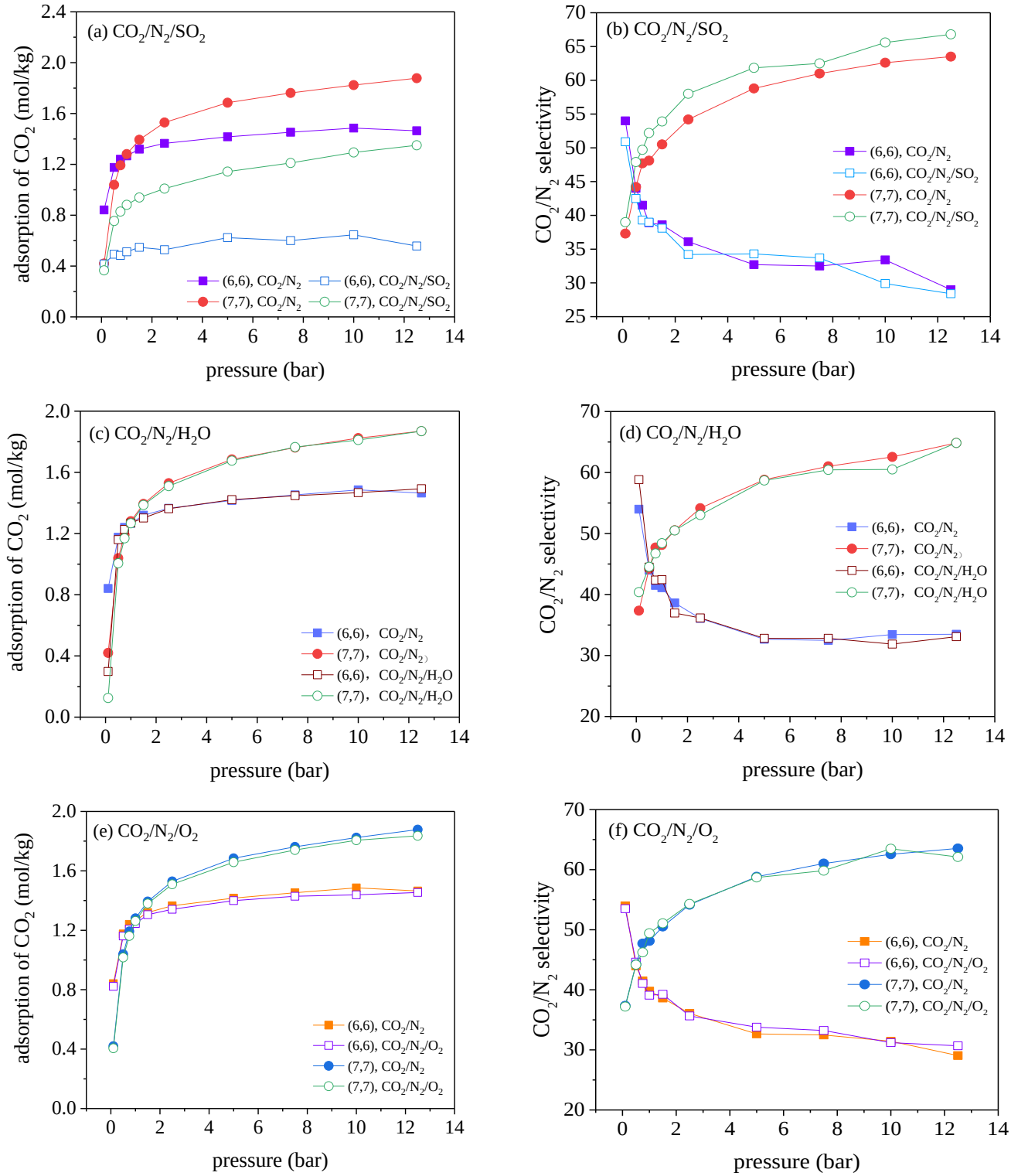

Figure 4. Adsorption isotherms for CO_2 in the presence of impurities, (**a**) SO_2, (**c**) H_2O, and (**e**) O_2, and (**b**,**d**,**f**) the corresponding CO_2/N_2 selectivity in the (6, 6) and (7, 7) CNTs, respectively.

To quantify the inhibition effect of impurity gas on the adsorption of CO_2, an inhibition coefficient is defined as

$$I = (a_b - a_{im})/a_b \times 100\% \quad (3)$$

where a_b and a_{im} represents the adsorbed amounts of CO_2 for the binary CO_2/N_2 mixture and for the ternary $CO_2/N_2/X$ mixture, respectively. As suggested, for the impure gas SO_2,

the inhibition coefficient in the (6, 6) CNT reaches up to 50.5%, 59.6%, and 61.9%, under the pressure of 0.1, 1.0, and 12.5 bar, respectively. Similarly, the inhibition coefficients in the (7, 7) CNT corresponds to 12.9%, 31.2%, and 28.1% under the same condition. However, as seen in Figure 4c, the impact of H_2O on the adsorption of CO_2 is significant at low pressure (0.1 bar), which yields an inhibition coefficient of 64.5%. When the pressure is increased to above 0.1 bar, the inhibition coefficient of H_2O sharply reduces to be negligible. It is interesting to find that both the adsorption of CO_2 and the CO_2/N_2 selectivity is barely affected by the presence of O_2 in the gas phase.

Figure 5a–c depicts the interactions of CO_2–CNT and of impurity gas X-CNT in the (6, 6) and (7, 7) CNTs. As given in Figure 5, it is evident that SO_2 has much stronger adsorption affinity with the nanotube wall than CO_2, so strong adsorptive competition between SO_2 and CO_2 occurs, associated with the adsorption space being favorably occupied by SO_2 molecules. Meanwhile, the interactions between CO_2 molecules and the nanotube wall becomes weaker due to the introduction of SO_2, so it is safe to conclude that the competitive adsorption and the weakened CO_2–CNT interactions are responsible for negative impacts on the adsorption of CO_2. Similar to the decreased adsorption of CO_2, the adsorption of N_2 also becomes smaller in the presence of SO_2 (see Figure S3 in Supplementary Materials).

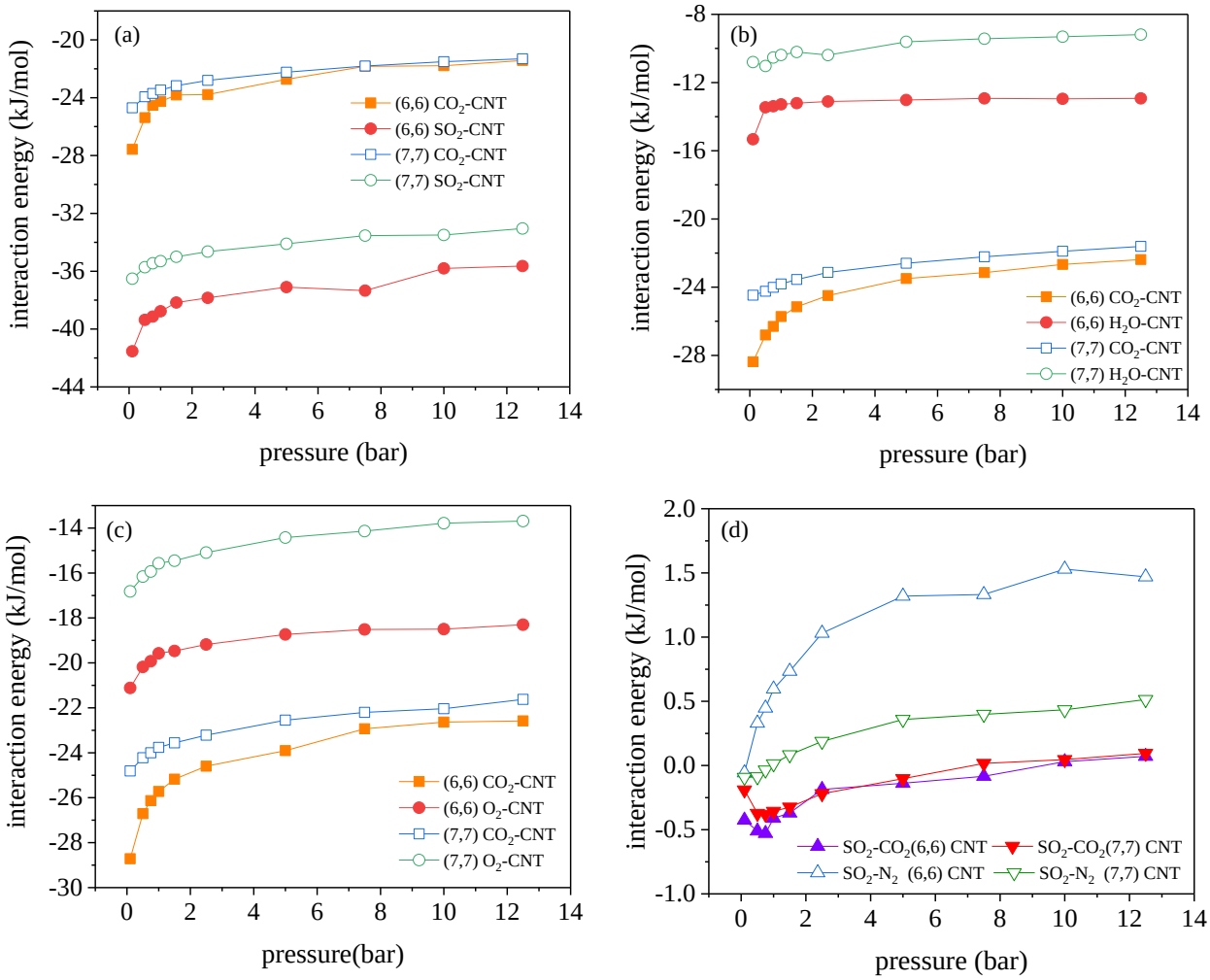

Figure 5. Variation of the interaction energies for CO_2–CNT and impurity–CNT including (**a**) SO_2–CNT, (**b**) H_2O–CNT and (**c**) O_2–CNT in the (6, 6) and (7, 7) CNTs with pressure. (**d**) The interaction energies of CO_2–SO_2 and N_2–SO_2 in the (6, 6) and (7, 7) CNTs for the $CO_2/N_2/SO_2$ mixtures, determined from GCMC simulations at 300 K.

In addition, although both the adsorption amounts of CO_2 and N_2 are decreased by the presence of SO_2 in the (6, 6) and (7, 7) CNTs, only a slight decrease in the CO_2/N_2 selectivity is found for (6, 6) CNT and the CO_2/N_2 selectivity is even enhanced in the (7, 7) CNT. To explain this phenomenon, the adsorbate–adsorbate interaction energies are estimated as a function of pressure for SO_2–CO_2 and SO_2–N_2 in Figure 5d. It is seen that CO_2 molecules are strongly attracted by the adsorbed SO_2 molecules in the (6, 6) and (7, 7) CNTs, whereas N_2 molecules suffer the strong repulsions from SO_2 molecules. As the additional CO_2–SO_2 interactions actually facilitate the selective adsorption of CO_2 over N_2, the CO_2/N_2 selectivity is enhanced by SO_2 in the (7, 7) CNT. However, the adsorbed SO_2 also enhances the entropic effect for CO_2 adsorbing in the (6, 6) CNT, further restricting the rotation freedom of CO_2 molecules, but this entropic effect exerts insignificant effect on the rotation of N_2 molecules. Although the adsorption of CO_2 is energetically favorable in the (6, 6) CNT in the presence of SO_2, the strengthened entropic effect has completely dominated over the energetic effect, thereby leading to the dramatically reduced CO_2 adsorption. The adsorption reduction arising from the dominant entropic effect is more significant for N_2 due to its unfavorable energetic field exerted by SO_2. Therefore, the CO_2/N_2 selectivity is reduced in the presence of SO_2 in the (6, 6) CNT.

Figure 4c indicates that, at the rather low pressure <0.1 bar (water vapor is at its saturation pressure, under a mole fraction of ~35.64%), noticeable adsorption of water vapor is found in the (6, 6) CNT, where considerable adsorption space is occupied. As depicted in Figure 6, the adsorption of water vapor decreases rapidly as a consequence of the competitive adsorption of CO_2 and N_2, where the corresponding partial pressures are enhanced at higher pressures. The inset of Figure 6 depicts the molecular configuration of water adsorbed in the (6, 6) CNT. As reported in the previous study, negligible adsorption of water was observed in the CNTs until the partial pressure of water vapor reached a critical pressure, where water molecules filled the CNT immediately and completely once the partial pressure was above the critical pressure [12,44]. It is shown that the critical pressure for the (6, 6) CNT is around the saturation pressure of water at 300 K, which is increased to 1.75 times of the saturation pressure in the (7, 7) CNT. Based on this reason, negligible adsorption of water is observed in the (7, 7) CNT within the pressure range investigated, while the effect of water vapor is only significant at rather low pressure in the (6, 6) CNT.

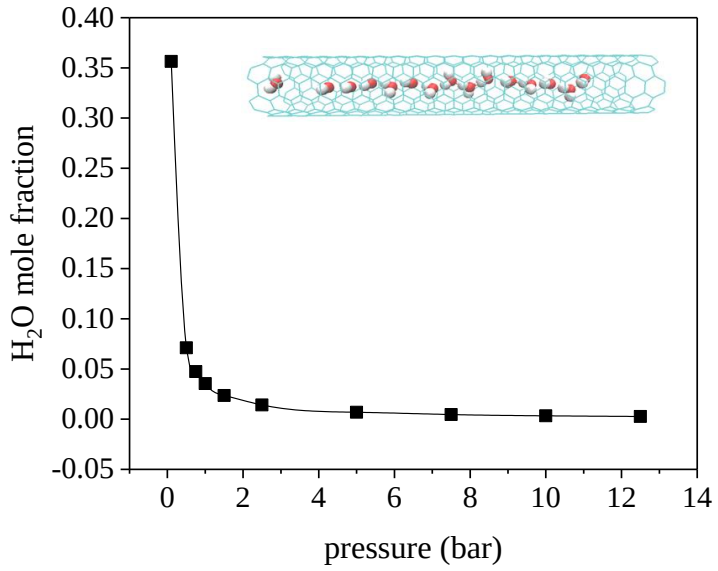

Figure 6. Variation of the H_2O mole ratio with total pressure of $CO_2/N_2/H_2O$ mixture, with the partial pressure of H_2O fixed at the saturation vapor pressure. The inset depicted a snapshot of the distribution of water in (6, 6) CNT at 0.1 bar and 300 K, in which a one-dimensional chain was evidently obtained.

Figure 4e,f depicts the adsorption isotherms for CO_2 and CO_2/N_2 selectivity in the presence of O_2 in the (6, 6) and (7, 7) CNTs, where both the adsorbed amounts and the CO_2/N_2 selectivity are hardly affected. This result can be explained by the analysis of the interaction energy between guest molecules and CNTs. As given in Figure 5c, the interactions of O_2–CNT are much stronger than the counterparts of N_2–CNT, so the competitive adsorption occurs between O_2 and N_2, leading to an enhanced CO_2/N_2 selectivity. However, the concentration of O_2 in the gas phase is only 4%, far below the mole concentration of N_2, 84% of N_2. Therefore, no significant decreases in adsorption of N_2 occurred, which is also applicable to the result for CO_2. A similar result is found in ZIF-68: the presence of O_2 has a negligible effect on CO_2 adsorption [12].

Apparently, the presence of impurity gas generally imposes a negative effect on the adsorption of CO_2, particularly in the rather small CNTs. However, the CO_2/N_2 selectivity demonstrates a complex dependency on the impure gases, which can be enhanced, reduced, or nearly unaffected. Meanwhile, both the adsorption of CO_2 and the CO_2/N_2 selectivity remain almost unaffected in the larger (10, 10) and (12, 12) CNTs, making it difficult to predict the optimal CNT with the highest separation performance. Therefore, it is necessary to introduce the performance coefficient, λ_e, which comprehensively evaluates the effect of the CO_2 adsorption and the CO_2/N_2 selectivity on the separation performance, by following

$$\lambda_e = \exp\left[\ln\left(\alpha_1 \frac{M_t}{M_p}\right) + \ln\left(\alpha_2 \frac{S_t}{S_p}\right)\right] \tag{4}$$

where M_t and S_t denote the adsorption of CO_2 and the CO_2/N_2 selectivity for the CNT of interest at the target pressure, respectively, while M_p and S_p represent the adsorption of CO_2 and the CO_2/N_2 selectivity for the standard case, respectively, which are chosen as the adsorption of CO_2 and the CO_2/N_2 selectivity of the (7, 7) CNT at 300 K and 1.0 bar. α_1 and α_2 are the weight factor s, which are set as 1.0 in this work.

Figure 7 illustrates the variation of the performance coefficient versus pressure in the (6, 6) CNT and (7, 7) CNT. As suggested, the performance coefficient is slightly increased in the (7, 7) CNT, while it becomes significantly decreased in the (6, 6) CNT. It is seen that SO_2 exhibits the most influential impact on the adsorption of CO_2 among the three impure gases considered. More specifically, the presence of SO_2 dramatically reduces the performance coefficient in the (6, 6) CNT, which is 180% lower than the results for CO_2/N_2 mixture. This is caused by the strong competitive adsorption between SO_2 and CO_2. For the impurities of H_2O and O_2, the changes in performance coefficient are generally negligible, except for the results of $CO_2/N_2/H_2O$ mixture at 1 bar. Based on the above results, it is readily derived that the influence of impurities on the CO_2 adsorption in CNTs followed the pattern: $SO_2 > H_2O > O_2$. Figure 7 indicates that, in the presence of impurities, the (6, 6) CNT still provides better performances for CO_2 capture than other CNTs when the pressures are below 0.5 bar, while the (7, 7) CNT exhibits the superior performance at higher pressures.

Additionally, we explored the adsorptive separation performance of CNTs for capturing SO_2 from the $CO_2/N_2/SO_2$ mixture by measuring the isotherm curve of SO_2 and the SO_2/N_2 selectivity, which are depicted in Figure 8. It should be pointed out that the (6, 6) CNT with a diameter of 0.81 nm exhibits outstanding performance for separation of SO_2/N_2, in which the maximum adsorbed amounts of SO_2 and the highest selectivity are achieved among the CNTs considered. More specifically, the SO_2/N_2 selectivities are unprecedentedly high, reaching 16,796, 13,965 and 7892 at the pressures of 0.1, 1.0 and 12.5 bar at 300 K, in the (6, 6) CNT.

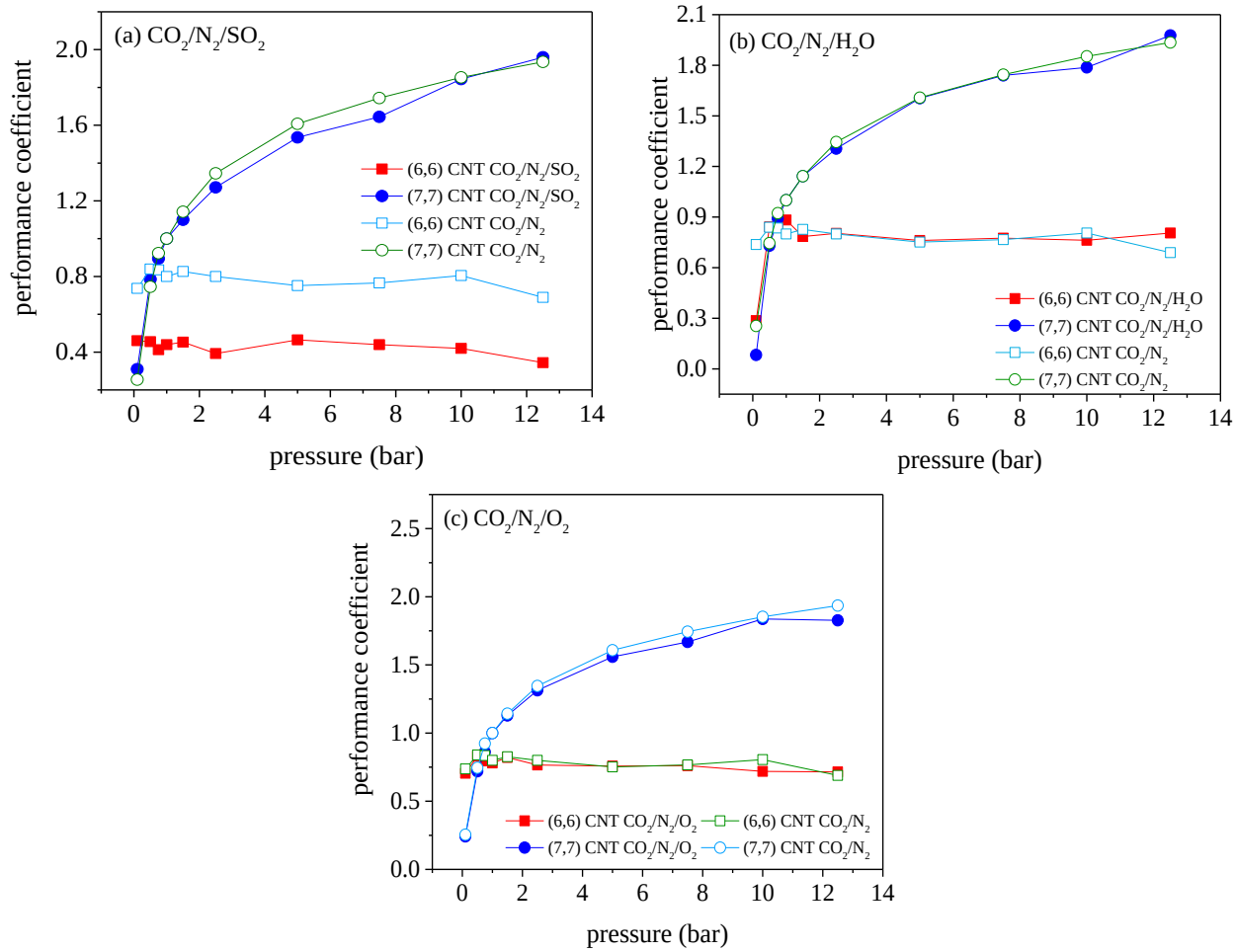

Figure 7. Variation of the performance coefficients of different CNTs in the presence of SO_2 (**a**), H_2O (**b**), and O_2 (**c**), relative to the adsorption of binary CO_2/N_2 mixture (CO_2/N_2 is 16/84) in the (7, 7) CNT at 1.0 bar and 300 K.

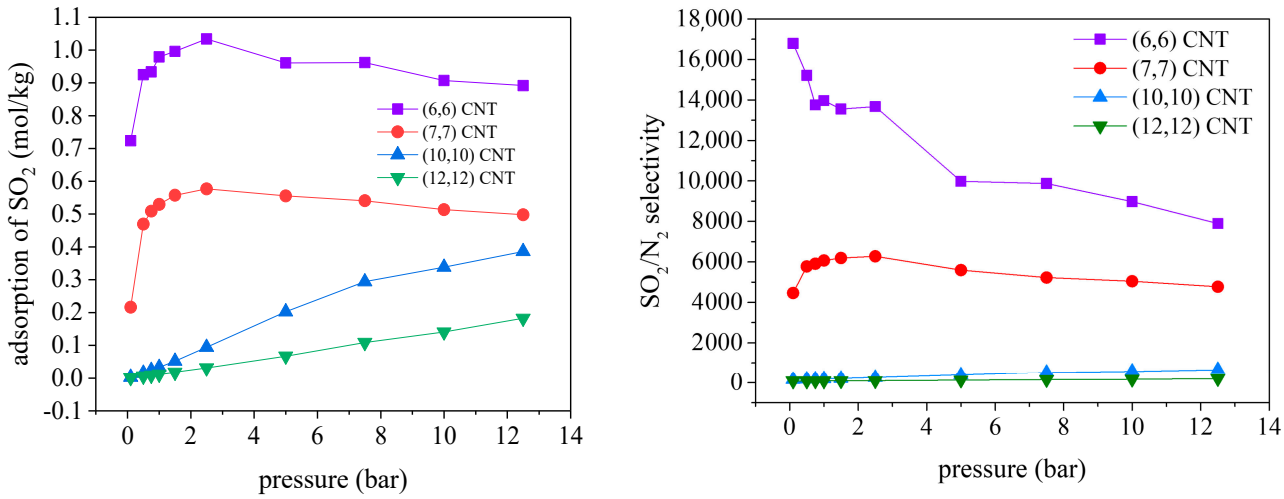

(**a**) (**b**)

Figure 8. Adsorption of (**a**) SO_2 and (**b**) SO_2/N_2 selectivity for the $CO_2/N_2/SO_2$ in CNTs with diameter varied from 0.807 to 1.626 nm at 300 K.

3.3. Impacts of Impurities on CO_2 Capture in Functionalized CNT Arrays

From the previous simulation results, it is evident that SO_2, as a polar molecule, yielded the strongest interaction with CNT, exerting the greatest impact on CO_2/N_2 adsorption and separation. As there are more complex interactions between impurities, it is interesting to explore the cooperative impact on the adsorption of CO_2 in this part. Due to the hydrophobicity of carbon nanotubes, the adsorption of water molecules is weak, and a small amount of H_2O barely affects the adsorption and separation of CO_2/N_2. In order to further explore the effect of H_2O on CO_2/N_2 adsorption, the hydrophilic carboxyl modified CNT is studied. In order to keep the same number of carboxyl groups distributed on the unit cell of CNT with different diameters, the mass fraction of carboxyl group doping is about 5.01–9.64%. After structure optimization by DFT, a 2×2 carbon nanotube array is constructed. When the tube spacing is set at 0.6 nm, GCMC is used to simulate the gas adsorption in carbon nanotube arrays with different diameters, using a fixed temperature and gas composition. After simulation, the adsorption configurations inside and outside the carbon nanotubes are calculated, respectively.

Figure 9 depicts the adsorption curves of CO_2 and N_2 and CO_2/N_2 selectivity mixed with impurity gases in four kinds of carbon nanotube arrays with tube spacing of 0.6 nm and temperature of 300 K. For CO_2/N_2 mixture, the optimal diameter of CNT bundle for adsorption separation of CO_2 is found in the (6, 6) CNT, which is different from the result based on single CNT. This is because (6, 6) CNT not only has the strongest adsorbate CNT interaction, but also can provide additional adsorption space between tubes, so the adsorption capacity becomes enhanced. Under the combined effect of the two factors, (6, 6) CNT array has the best adsorption capacity and CO_2/N_2 selectivity under 10 bar. At higher pressure, due to the limited adsorption space, the adsorption capacity becomes lower than that for the (7, 7) CNT array. Compared with the binary mixture, the adsorption capacity of CO_2 and N_2 in quinary mixture is severely inhibited, especially in the small diameter (6, 6) CNT array, but the adsorption capacity of CO_2 and N_2 in the (7, 7) CNT array is the highest below 1 bar. In the (10, 10) and (12, 12) CNT arrays with large diameters, the adsorption capacity of CO_2 increases almost linearly with the pressure, which becomes dominant when the pressure is greater than 1 bar. In addition, the CO_2/N_2 selectivity of the quinary mixture is increased. In particular, for (7, 7) CNT arrays, the adsorption capacity of CO_2 and N_2 decreased by 2.28 times and 4.45 times at 1 bar, respectively, but the selectivity increased by 1.95 times. This is because the inhibition effect is stronger for N_2 (nonpolar molecule), in comparison with CO_2. In addition, the selectivity of CO_2/N_2 in the quinary mixture is increased. By calculating the performance coefficient, as shown in Figure 10, it is found that (7, 7) CNT array always maintains the best adsorption separation performance, except some results at a very low pressure of 0.1 bar.

In order to explore the inhibition mechanism in the CNT array with a small diameter, the adsorption ratio inside and outside the CNT (amount adsorbed inside the CNT/adsorption amount outside the CNT) is calculated. According to Figure 11 plotted the ratio of internal and external adsorption capacity for binary and quinary mixtures. As suggested, in the binary mixture, CO_2 and N_2 tend to be trapped by the outside of the tube in the small diameter, except some measurements at the pressure below 1 bar. This is due to the strong interaction between adsorbate and CNT in the small diameter below 1 bar. With increase in sorbate loading, the adsorption space in the tube is limited, so a large amount of adsorbate is captured by the outside of the tube. However, the interaction between adsorbate and CNT is weak in CNT with large diameter, so CO_2 molecules tend to be adsorbed outside the tube. In the quinary mixture, the adsorption distribution of CO_2 molecules is more complex. In the (12, 12) CNT array, CO_2 molecules begin to be adsorbed mainly in the tube, which is distributed uniformly outside the tube with pressure. With the increase in the pressure, the pressure in the tube becomes dominant.

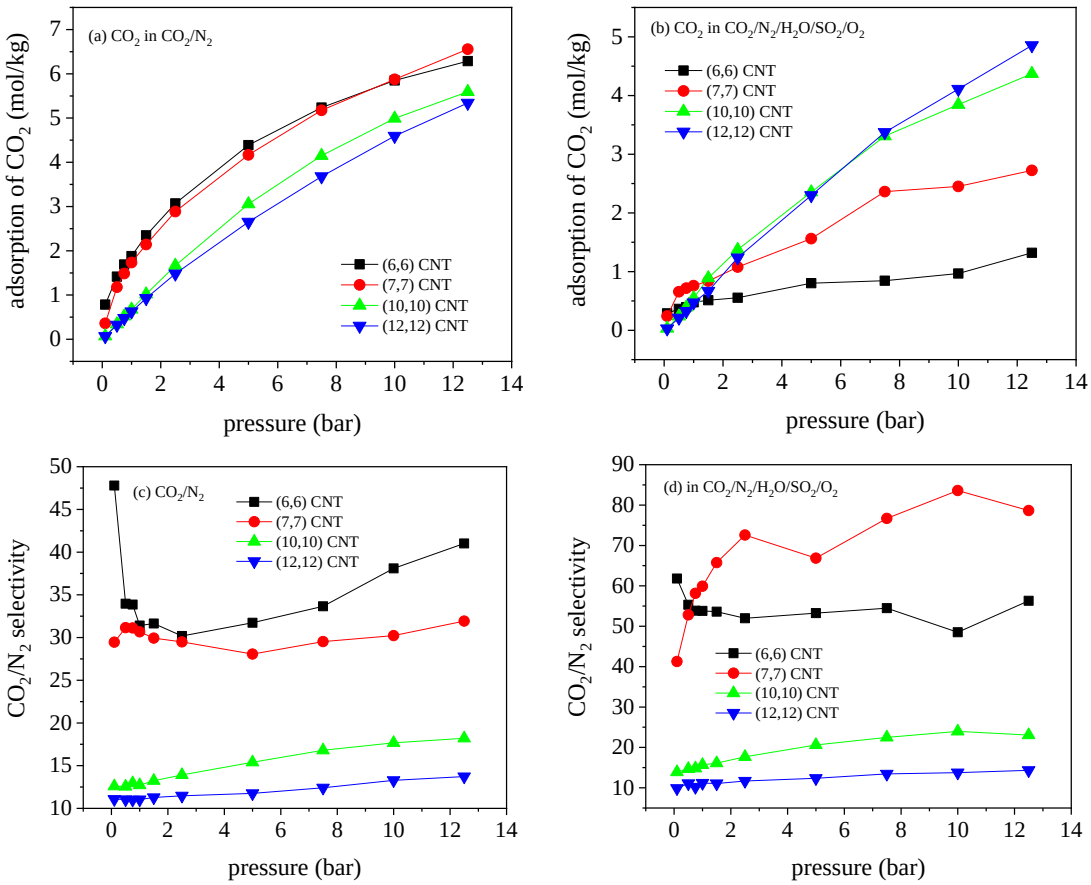

Figure 9. Adsorption isothermal curves of CO_2 in (**a**) CO_2/N_2 mixture and (**b**) quinary mixture, as well as the corresponding CO_2/N_2 selectivities for (**c**) CO_2/N_2 mixture and (**d**) quinary mixture.

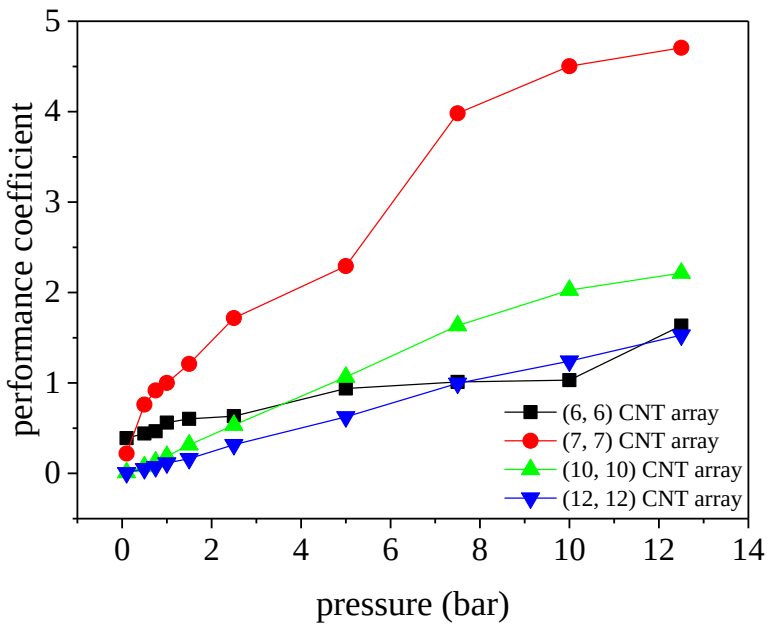

Figure 10. Performance coefficients of CO_2/N_2 adsorption and separation of quinary mixtures in modified CNTs with different diameters.

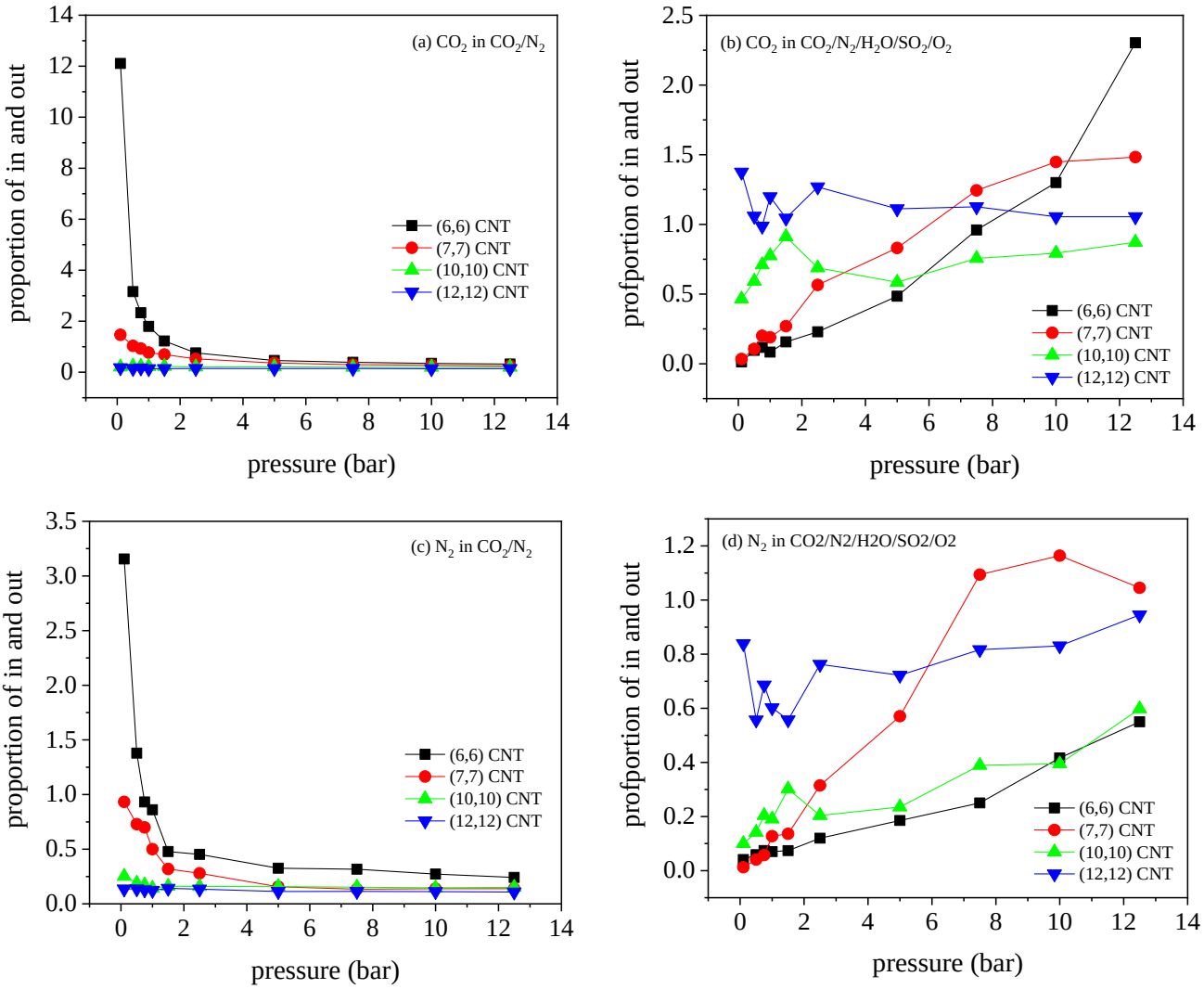

Figure 11. The ratio of adsorption capacity of (**a**,**b**) CO_2 and (**c**,**d**) N_2 in binary and quinary mixtures inside and outside the CNT arrays, with four different diameters.

The isothermal curves of water molecules and SO_2 in the modified CNTs are plotted in Figure 12, where the adsorption capacity of water molecules after carboxyl modification is greatly improved. The adsorption is mainly distributed between tubes, while the adsorption capacity inside tubes is almost zero. According to the molecular snapshot of water molecules adsorbed in (7, 7) CNT array in Figure 13, a large number of water molecules are adsorbed and aggregated between tubes to form chain structures, but the adsorption of water molecules in tubes is hardly observed. At the same time, the adsorption capacity of water molecules decreases with the increase in tube diameter. By calculating the mass fraction of doping carboxyl, it is found that the carboxyl content is an important factor to affect the adsorption capacity of water molecules. As the diameter of the tube increased, the mass fraction of carboxyl group decreases, leading to the decrease in the adsorption capacity of water molecules. The presence of water molecules promotes the adsorption of SO_2 in the small-diameter nanotube arrays. In Figure 14, the results for interaction energy of H_2O–SO_2 indicate in the small-diameter (6, 6) and (7, 7) CNTs, SO_2 is subject to stronger H_2O–SO_2 interaction than CO_2–H_2O, thereby enhancing the adsorption of SO_2.

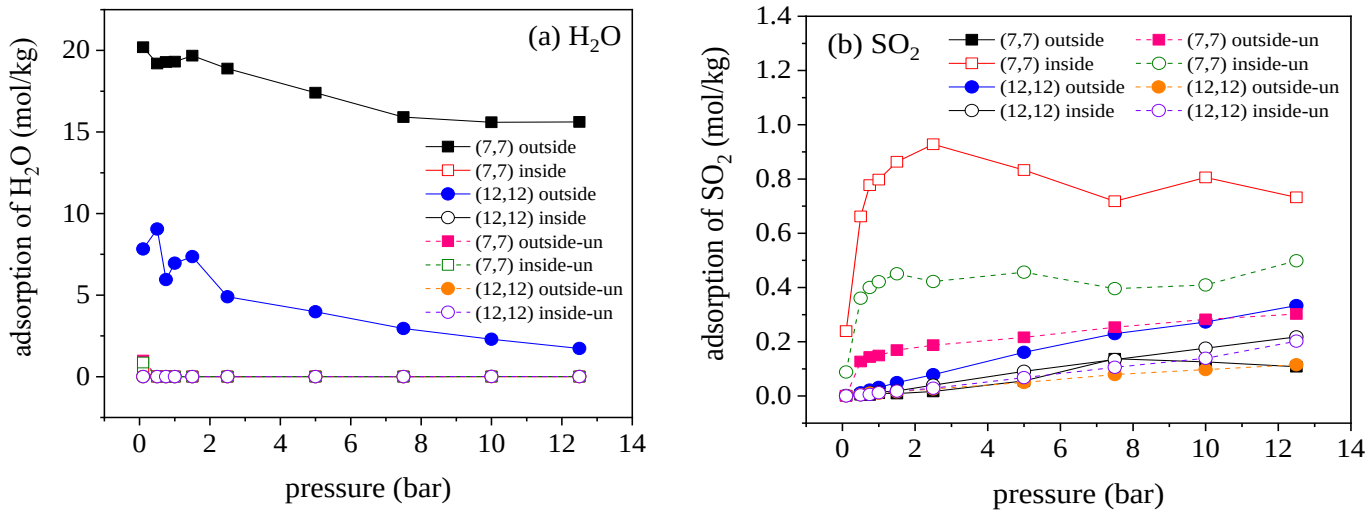

Figure 12. Isothermal adsorption curves of water molecules (**a**) and SO_2 (**b**) inside and outside the tube in unmodified and modified CNT array.

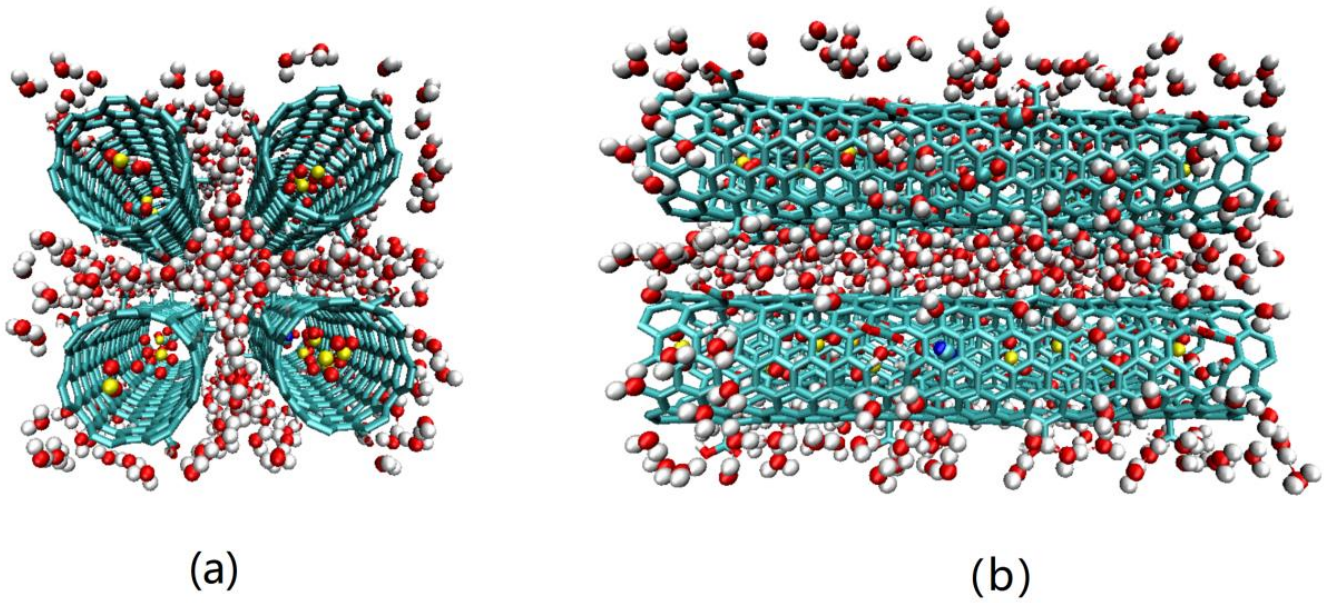

Figure 13. Molecular snapshot of (7, 7) CNT array in cross section (**a**) and axial direction (**b**) at 1.0 bar, 300 K.

In the modified CNTs, carboxyl group has little effect on the adsorption of adsorbate molecules. By simulating the adsorption of quinary mixture in a single carboxyl modified CNT, the results show that the adsorption capacity of various adsorbents is reduced, in comparison with the simulation results for unmodified CNTs. This is due to the introduction of defect groups (or the lack of carbon atoms) which weaken the interaction between the adsorbate molecules and the wall of small-diameter CNTs, so the adsorption capacity is reduced. The introduction of carboxyl group barely promotes the adsorption and separation coefficient of adsorbate molecules in the carbon tubes, suggesting that H_2O plays an important role in the adsorption capacity and distribution of CO_2.

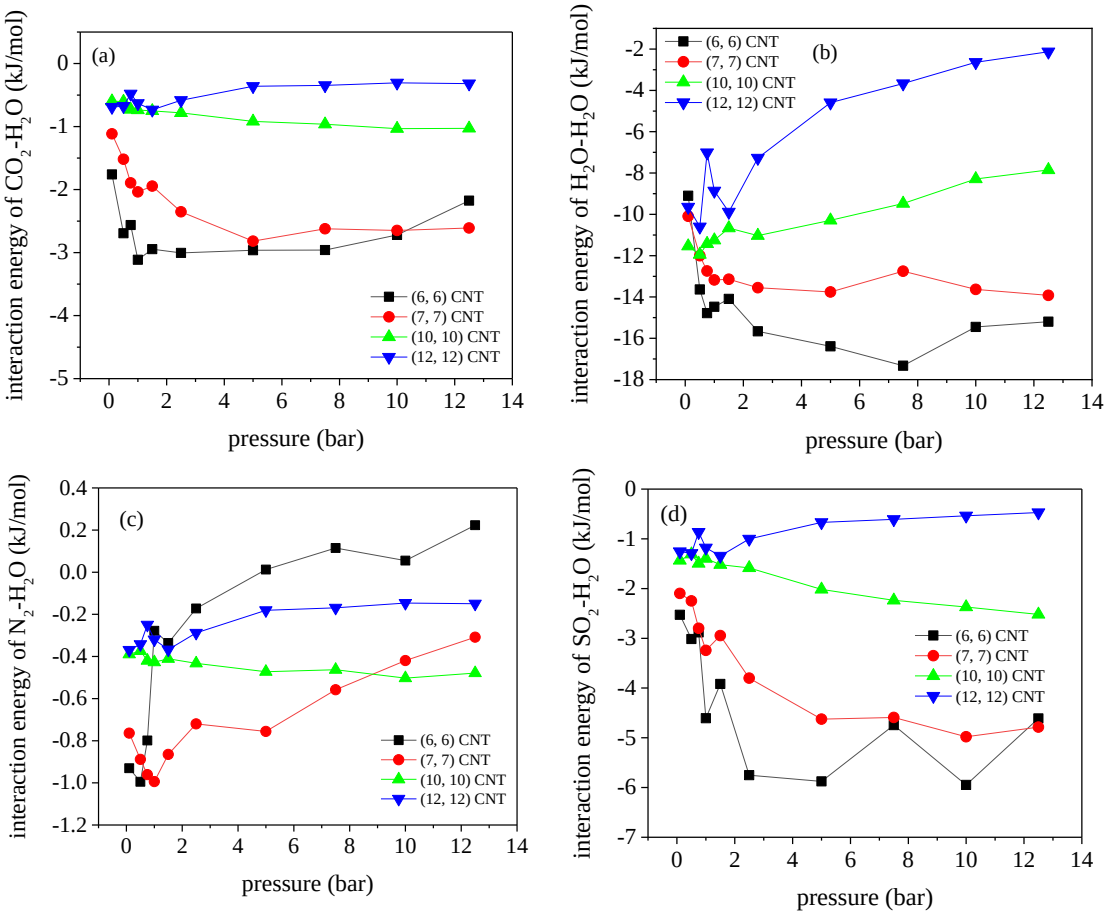

Figure 14. Interaction energy of CO_2-H_2O (**a**), H_2O-H_2O (**b**), N_2-H_2O (**c**) and H_2O-CO_2 (**d**) in CNT arrays with four diameters.

The adsorption of CO_2 and N_2 in the quinary mixture outside the tube is seriously inhibited, but the inhibition or promotion for adsorption inside the tube varies with nanotubes with different diameters. As the carboxyl functional group hardly exerts a positive effect on the adsorption of CO_2 molecules in the tube, the adsorption of CO_2 molecules in the tube is mainly affected by the interaction with other adsorbate molecules. Due to the large amount of adsorbed water molecules between the small nanotubes, the adsorption of CO_2 molecules mainly occurs in the tube. However, at low pressures, the adsorption of SO_2 in the tube is enhanced due to the presence of H_2O. Meanwhile, the adsorption of CO_2 in the tube is strongly inhibited by the intensive competitive adsorption, so CO_2 adsorption mainly occurs outside the tube at low pressures. According to the previous simulation results of $CO_2/N_2/SO_2$ mixture in a single CNT, SO_2 has little effect on the adsorption of CO_2 in a large diameter tube, so CO_2 is mainly adsorbed in the tube at low pressure. With the increase in pressure, the adsorption amount of H_2O outside the tube decreases, where the inhibition effect weakens, so CO_2 molecules begin to adsorb outside the tube, and are finally evenly distributed inside and outside the tube. In addition, the adsorption enthalpy of CO_2 is increased by the attraction of H_2O–CO_2 in the tube, where the adsorption space is abundant in the large diameter tube, so the adsorption of CO_2 increases.

As derived from the previous analysis, SO_2 can enhance the selectivity of CO_2/N_2 in the small diameter. In addition, CO_2 is subject to stronger interaction from H_2O than N_2, so the presence of water can also promote the CO_2/N_2 selectivity. The selectivity of CO_2/N_2 in the small diameter is increased by the combination of the two impure gases. In particular, at 1 bar, the CO_2/N_2 selectivity of (6, 6) CNT array increases from 30.4 to 53.8, while an increase from 30.7 to 59.9 are found for (7, 7) CNT array. The growth ratio corresponds to 1.77 and 1.95 times, respectively. As the adsorption space in (6, 6) CNT

array is very small, the derived adsorption capacity of CO_2 is also very limited due to the competitive adsorption of H_2O and SO_2. For (7, 7) CNT array, the adsorption space is promoted, so the adsorption capacity of CO_2 in (7, 7) CNT array becomes higher than that in (6, 6) CNTs. As the inhibition of CO_2 in (7, 7) CNTs is weaker than that in (6, 6) CNT array, the selectivity of CO_2/N_2 is higher. To sum up, the adsorption of H_2O molecules mainly occurs between tubes, thereby inhibiting the adsorption of CO_2 between tubes, while SO_2 molecules compete with CO_2 molecules in tubes to induce the inhibition effect. The competition between the two effects determines the adsorption distribution of CO_2 inside and outside the tube. In addition, the interaction of H_2O and SO_2 improves the selectivity of CO_2/N_2, and the (7, 7) CNT array maintains the best CO_2/N_2 adsorption and separation performance except the results at low pressure of 0.1 bar.

4. Conclusions

In this work, a grand canonical Monte Carlo simulation is used to investigate the influence of impurity gases, including water, SO_2, and O_2, on the adsorption of CO_2 in singe CNTs and functionalized CNT bundles. Initially, the effect of pore size of CNT on the adsorption of CO_2/N_2 mixture is examined, and it is revealed that the adsorption capacity had a strong dependence on the CNT diameter. Further, the influence of single impure gas on the adsorption of CO_2 in CNTs is explored. By calculating inhibition coefficient to evaluate the influence on the adsorption of CO_2, results indicate that SO_2 is the most influential impure to affect the adsorption of CO_2/N_2. By introducing SO_2, the interaction of CO_2-CNT became weaker. Meanwhile, SO_2 could compete with CO_2 for the adsorption site, which exerts a negative effect on the adsorption of CO_2, so the adsorption amount of CO_2 has a significant decrease. Furthermore, the (6, 6) CNT exhibits superior performance for adsorption separation of SO_2/N_2. As for H_2O, due to the partial pressure decreases sharply with pressure, decrease on the adsorption of CO_2 only occurs noticeably bellow 0.1 bar. The existence of O_2 hardly changes the adsorption amounts andthe CO_2/N_2 selectivity. Moreover, the performance coefficient is calculated to evaluate the adsorptive separation of CO_2 comprehensively. It is shown that SO_2 was the most influential impure gas to affect the adsorptive separation of CO_2 from flue mixture. Eventually, the coexisting influence of three impure gases is also investigated. The performance coefficient is also calculated for the complex correlation with the diameter; however, it is hardly affected by the complex interaction among adsorbates. Among our simulations, the (7, 7) CNT yields the superior performance for CO_2 adsorption and separation, where both the maximum uptakes and the highest selectivity occurs to the ambient temperature and pressure.

Supplementary Materials: The following supporting information can be downloaded online. Figure S1: Adsorption isotherms for CO_2 in the presence of impurities, (a) SO_2, (c) H_2O, and (e) O_2, and the corresponding CO_2/N_2 selectivity (b, d and f), in the (10, 10) and (12, 12) CNTs. Figure S2: Isotherm curves with pressure for (a) SO_2 in $CO_2/N_2/SO_2$, (b) H_2O in $CO_2/N_2/H_2O$, and (c) O_2 in $CO_2/N_2/O_2$, in (6, 6), (7, 7), (10, 10) and (12, 12) CNTs at temperature of 300 K. Figure S3: The adsorption of N_2 in the presence of impurities which are (a, b) SO_2, (c, d) H_2O and (e, f) O_2. The leaf side is these mixtures in the (6, 6) and (7, 7) CNTs, and the right side is that in (10, 10) and (12, 12) CNTs. Figure S4: Variation interaction energy of X-CNT which X represents SO_2, H_2O and O_2 with pressure in the (10, 10) (a) and (12, 12) (b) CNTs.

Author Contributions: Conceptualization, S.L. and Y.S.; methodology, Y.S.; software, Y.S.; validation, Y.S., S.L. and X.G.; investigation, S.L.; writing—original draft preparation, Y.S.; writing—review and editing, X.G.; visualization, Y.S.; supervision, S.L.; project administration, S.L. All authors have read and agreed to the published version of the manuscript.

Funding: This research was funded by the Fundamental Research Funds for the Central University (grant number 2021CDJQY-029), State Key Laboratory of Pollution Control and Resource Reuse for the Open Fund support (grant number PCRRF19038) and China Postdoctoral Science Foundation (grant number 2021M690175).

Institutional Review Board Statement: Not applicable.

Informed Consent Statement: Not applicable.

Data Availability Statement: The data presented in this study are available on request from the corresponding authors.

Conflicts of Interest: The authors declare no conflict of interest.

References

1. Yu, J.; Ma, Y.; Balbuena, P.B. Evaluation of the impact of H_2O, O_2, and SO_2 on postcombustion CO_2 capture in metal-organic frameworks. *Langmuir* **2012**, *28*, 8064–8071. [CrossRef]
2. Younas, M.; Sohail, M.; Leong, L.K.; Bashir, M.J.; Sumathi, S. Feasibility of CO_2 adsorption by solid adsorbents: A review on low-temperature systems. *Int. J. Environ. Sci. Technol.* **2016**, *13*, 1839–1860. [CrossRef]
3. Liu, L.; Bhatia, S.K. Molecular Simulation of CO_2 Adsorption in the Presence of Water in Single-Walled Carbon Nanotubes. *J. Phys. Chem. C* **2013**, *117*, 13479–13491. [CrossRef]
4. Rende, D.; Ozgur, L.; Baysal, N.; Ozisik, R. A Computational Study on Carbon Dioxide Storage in Single Walled Carbon Nanotubes. *J. Comput. Theor. Nanosci.* **2012**, *9*, 1658–1666. [CrossRef]
5. Siriwardane, R.V.; Shen, M.S.; Fisher, E.P.; Poston, J.A. Adsorption of CO_2 on Molecular Sieves and Activated Carbon. *Energy Fuels* **2001**, *15*, 279–284. [CrossRef]
6. Cheng, Y.; Huang, Q.; Eic, M.; Balcom, B.J. CO_2 dynamic adsorption/desorption on zeolite 5A studied by 13C magnetic resonance imaging. *Langmuir* **2005**, *21*, 4376–4381. [CrossRef]
7. Gao, W.; Butler, D.; Tomasko, D.L. High-pressure adsorption of CO_2 on NaY zeolite and model prediction of adsorption isotherms. *Langmuir* **2004**, *20*, 8083–8089. [CrossRef]
8. Millward, A.R.; Yaghi, O.M. Metal-Organic Frameworks with Exceptionally High Capacity for Storage of Carbon Dioxide at Room Temperature. *Am. Chem. Soc.* **2005**, *127*, 17998–17999.
9. Chen, H.; Johnson, J.K.; Sholl, D.S. Transport Diffusion of Gases Is Rapid in Flexible Carbon Nanotubes. *J. Phys. Chem. B* **2006**, *110*, 1971–1975. [CrossRef]
10. Skoulidas, A.I.; Ackerman, D.M.; Johnson, J.K.; Sholl, D.S. Rapid transport of gases in carbon nanotubes. *Phys. Rev. Lett.* **2002**, *89*, 185901. [CrossRef]
11. Liu, L.; Nicholson, D.; Bhatia, S.K. Adsorption of CH_4 and CH_4/CO_2 mixtures in carbon nanotubes and disordered carbons: A molecular simulation study. *Chem. Eng. Sci.* **2015**, *121*, 268–278. [CrossRef]
12. Liu, L.; Nicholson, D.; Bhatia, S.K. Impact of H_2O on CO_2 Separation from Natural Gas: Comparison of Carbon Nanotubes and Disordered Carbon. *J. Phys. Chem. C* **2014**, *119*, 407–419. [CrossRef]
13. Liu, L.; Nicholson, D.; Bhatia, S.K. Exceptionally high performance of charged carbon nanotube arrays for CO_2 separation from flue gas. *Carbon* **2017**, *125*, 245–257. [CrossRef]
14. Liu, L.; Hu, C.; Nicholson, D.; Bhatia, S.K. Inhibitory Effect of Adsorbed Water on the Transport of Methane in Carbon Nanotubes. *Langmuir* **2017**, *33*, 6280–6291. [CrossRef]
15. Lin, Z.; Liu, C.; Liu, L.; He, D.; Wang, X.; Zhou, X.; Zhang, Y. Unprecedentedly high selective adsorption of Xe/Kr mixtures in carbon nanotubes: A molecular simulation study. *Chem. Eng. J.* **2020**, *393*, 124744. [CrossRef]
16. Liu, L.; Nicholson, D.; Bhatia, S.K. Effects of Flange Adsorption Affinity and Membrane Porosity on Interfacial Resistance in Carbon Nanotube Membranes. *ACS Appl. Mater. Interfaces* **2018**, *10*, 34706–34717. [CrossRef]
17. Liu, L.; Nicholson, D.; Bhatia, S.K. Interfacial Resistance and Length-Dependent Transport Diffusivities in Carbon Nanotubes. *J. Phys. Chem. C* **2016**, *120*, 26363–26373. [CrossRef]
18. Liu, L.; Bhatia, S.K. Influence of Morphology on Transport Properties and Interfacial Resistance in Nanoporous Carbons. *J. Phys. Chem. C* **2019**, *123*, 21050–21058. [CrossRef]
19. Wang, Q.; Liu, L.; Liu, C.; Song, J.; Gao, X. Size effect in determining the water diffusion rate in carbon nanotubes. *J. Mol. Liq.* **2021**, *334*, 116034. [CrossRef]
20. Song, J.; Liu, L.; Li, Q.; Liu, C.; Song, F. Entrance resistance of water transport into carbon nanotubes: Insights from molecular dynamics simulations. *J. Mol. Liq.* **2021**, *331*, 115739. [CrossRef]
21. Lin, Z.; Liu, L.; Liu, C.; Liu, Y. Optimal Performance of Nanoporous Carbons on Adsorptive Separation of CO_2 from Flue Gas. *Energy Fuels* **2021**, *35*, 8069–8080. [CrossRef]
22. Song, J.; Liu, L.; Liu, C.; Gao, X. Interfacial resistance of gas transport through rigid and flexible zeolites. *Sep. Purif. Technol.* **2021**, *278*, 119529. [CrossRef]
23. Wang, Q.; Liu, L.; Han, L.; Liu, C.; Liu, Y. Exchange dynamics of molecules at the fluid-solid interface determining the diffusion rate in nanopores. *J. Mol. Liq.* **2021**, *335*, 116030. [CrossRef]
24. Lin, Z.; Liu, L.; Liu, C.; Gao, X. Adsorptive separation of Xe/Kr using nanoporous carbons in the presence of I_2 and CH_3I. *Sep. Purif. Technol.* **2021**, *275*, 119161. [CrossRef]
25. Lee, K.B.; Sircar, S. Removal and recovery of compressed CO_2 from flue gas by a novel thermal swing chemisorption process. *AIChE J.* **2008**, *54*, 2293–2302. [CrossRef]
26. Liu, J.; Wei, Y.; Zhao, Y. Trace Carbon Dioxide Capture by Metal–Organic Frameworks. *ACS Sustain. Chem. Eng.* **2018**, *7*, 82–93. [CrossRef]

27. Chang, S.-C.; Chien, S.-Y.; Chen, C.-L.; Chen, C.o.-K. Analyzing adsorption characteristics of CO_2, N_2 and H_2O in MCM-41 silica by molecular simulation. *Appl. Surf. Sci.* **2015**, *331*, 225–233. [CrossRef]
28. Kowalczyk, P. Molecular insight into the high selectivity of double-walled carbon nanotubes. *Phys. Chem. Chem. Phys.* **2012**, *14*, 2784–2790. [CrossRef]
29. Li, G.; Xiao, P.; Webley, P.A.; Zhang, J.; Singh, R. Competition of CO_2/H_2O in adsorption based CO_2 capture. *Energy Procedia* **2009**, *1*, 1123–1130. [CrossRef]
30. Jia, W.; Murad, S. Separation of gas mixtures using a range of zeolite membranes: A molecular-dynamics study. *J. Chem. Phys.* **2005**, *122*, 234708. [CrossRef]
31. Zhang, J.; Zou, H.L.; Qing, Q.; Yang, Y.L.; Li, Q.W.; Liu, Z.F.; Guo, X.Y.; Du, Z.L. Effect of chemical oxidation on the structure of single-walled carbon nanotubes. *J. Phys. Chem. B* **2003**, *107*, 3712–3718. [CrossRef]
32. Hu, H.; Zhao, B.; Itkis, M.E.; Haddon, R.C. Nitric acid purification of single-walled carbon nanotubes. *J. Phys. Chem. B* **2003**, *107*, 13838–13842. [CrossRef]
33. Daley, M.A.; Mangun, C.L.; DeBarrb, J.A.; Riha, S.; Lizzio, A.A.; Donnals, G.L.; Economy, J. Adsorption of SO_2 onto oxidized and heat-treated activated carbon fibers (ACFS). *Carbon* **1997**, *35*, 411–417. [CrossRef]
34. Picaud, S.; Collignon, B.; Hoang, P.N.; Rayez, J.C. Adsorption of water molecules on partially oxidized graphite surfaces: A molecular dynamics study of the competition between OH and COOH sites. *Phys. Chem. Chem. Phys.* **2008**, *10*, 6998–7009. [CrossRef] [PubMed]
35. Harris, J.G.; Yung, K.H. Carbon Dioxide's Liquid-Vapor Coexistence Curve and Critical Properties As Predicted by a Simple Molecular Model. *J. Phys. Chem.* **1995**, *99*, 12021–12024. [CrossRef]
36. Potoff, J.J.; Siepmann, J.I. Vapor–liquid equilibria of mixtures containing alkanes, carbon dioxide, and nitrogen. *AIChE J.* **2001**, *47*, 1676–1682. [CrossRef]
37. Berendsen, H.J.C.; Grigera, J.R.; Straatsma, T.P. The Missing Term in Effective Pair Potentials. *J. Phys. Chem. C* **1987**, *91*, 6269. [CrossRef]
38. Sokolić, F.; Guissani, Y.; Guillot, B. Molecular dynamics simulations of thermodynamic and structural properties of liquid SO_2. *Mol. Phys.* **2006**, *56*, 239–253.
39. Maitland, G.; Rigby, M.; Smith, E.; Wakeham, W.; Henderson, D. Intermolecular Forces: Their Origin and Determination. *Phys. Today* **1983**, *36*, 57–58.
40. Tang, Y.W.; Chan, K.Y. The Dot and Line Method: A Long Range Correction to Coulomb Interaction in a Cylindrical Pore. *Mol. Simul.* **2004**, *30*, 63–70. [CrossRef]
41. Zhang, Q.; Chan, K.-Y.; Quirke, N. Molecular dynamics simulation of water confined in a nanopore of amorphous silica. *Mol. Simul.* **2009**, *35*, 1215–1223. [CrossRef]
42. Peng, D.-Y.; Robinson, D.B. A New Two-Constant Equation of State. *Ind. Eng. Chem. Fundam.* **1976**, *15*, 59–64. [CrossRef]
43. John, P.; Perdew, K.B. Generalized gradient approximation made simple. *Phys. Rev. Lett.* **1996**, *77*, 3865.
44. Liu, Y.; Liu, J.; Lin, Y.S.; Chang, M. Effects of Water Vapor and Trace Gas Impurities in Flue Gas on CO_2/N_2 Separation Using ZIF-68. *J. Phys. Chem. C* **2014**, *118*, 6744–6751. [CrossRef]